

Figure S1. Related to Figure 1; Assay metrics from ChIP-reporter STARR-seq experiments. (A) Fragment diversity as a function of read depth. The number of unique fragments from sequencing reads plotted as a function of the total number of reads. Number of fragments per library was estimated by B_{max} in a model that accounts for saturation and non-specific sequencing errors ($Y = B_{max} \cdot X / (K_d + X)$ active NS $\cdot X$ active Background). The diversity of fragments in the input library is indicated in red, where the dotted line is the fit model. The estimated model parameters and standard errors were: $B_{max} = 2.9 \times 10^6 \pm 1868$, $K_d = 2.9 \times 10^6 \pm 3329$, $NS = 0.029 \pm 1.1 \times 10^{-4}$, Background = -7910 ± 318.5 (B) Correlation between GR ChIP-seq and ChIP-reporter libraries across replicates. After alignment, the number of fragments aligning to each of the called GR binding sites was calculated. The libraries were then compared by correlating the per-binding-site fragment counts between libraries using a Spearman correlation. Plotted is a heat map of the correlations. (C) Distribution of fragment sizes as determined by paired-end sequencing in the input GR ChIP-seq library (black), the ChIP-reporter input library (blue), and the ChIP-reporter output library (red). The GR ChIP-seq and ChIP-reporter output libraries were generated from A549 cells after treatment for 3 h with 100 nM DEX. (D) Distribution of read depth across GR binding sites. The distribution of log-transformed read depth averaged across all ChIP-reporter output libraries is shown for all GR binding sites (black), the sites tested for response with DESeq2 (red), and the sites excluded from testing by DESeq2 (blue). (E) Distribution of DEX-response effect sizes in ChIP-reporter assays. The fold-change in ChIP-reporter activity between DEX and EtOH treatments was calculated for every tested GR binding site after normalizing the read depth for the total number of aligned reads. Plotted is the distribution of those values after performing a \log_2 transformation. The mean and median of the distribution was 0.20 and 0.28, respectively, and a heavy right tail (e.g. 1st quartile = -0.16, 3rd quartile = 0.64) indicates an overall prevalence of GR binding sites with increased activity after DEX treatment. (F) Negative binomial model of the mean-variance relationship using. To account for over dispersion in sequencing read counts, DESeq2 was used to fit a negative binomial model to estimate the relationship between mean sequencing depth at each GR binding site, and the dispersion in that site. The red line indicates the fit, and blue indicated the final dispersion estimates used in testing. (G) ChIP-reporter expression as a function of fragment size. All assayed DNA fragments were placed into three equal bins by fragment size. Sites were mapped to GR binding sites and bins were individually subsampled to normalize for number of fragments in each bin. DEX-inducible activity is plotted for each bin. (H) qPCR of STARR-seq transcript levels from a vector containing a DEX-responsive enhancer from the *PER1* locus. Cells were treated with medium containing 0.02% EtOH (3.5 h), 100 nM DEX (3.5 h) or with 100 nM DEX (0.5 h) and then washed with medium containing 0.02% EtOH and treated for an additional 3 h. Error bars indicate S.D. (I) Box plots of data from dual luciferase assays used to validate ChIP STARR-seq reporter experiments. Error bars indicate S.D.

Figure S2. Related to Figure 1; Nuclear plasmid abundance after hormone treatment is not influenced by the presence of DEX-inducible functional elements. (A) The DEX-inducible enhancer landscape of the *PER1* locus. Y-axis is $-\log_{10}(p \text{ value})$ from Wilcoxon rank sum test. (B, C) High-resolution view of chr17:8,055,091-8,055,366 and chr17:8,057,549-8,057,958 enhancer loci showing read-depth normalized mapped plasmid reads from purified nuclei isolated from cells transfected with GC-inducible STARR-seq libraries and treated with 100 nM DEX or 0.02% EtOH for 3 h (top six tracks), STARR-seq significance and ChIP peak location. No loci of ~1 Mb assayed had significant differences in nuclear-localized plasmid content between DEX and EtOH conditions.

Figure S3. Related to Figure 2; Direct GR binding sites confer DEX-inducible function

(A) Addition of GREs increases DEX-induced reporter gene expression from sites that are bound by the GR but are not induced in ChIP-reporter assays. (B) GRE prediction of DEX-induced ChIP-reporter activity as a function of FDR threshold. The GRE was used to predict positive DEX-responsiveness (i.e. increased activity after DEX treatment) in ChIP-reporter assays across a range of ChIP-reporter FDR thresholds. For each FDR threshold (x-axis), the AUC for the resulting ROC curve is shown. Red points are for the experimental data, and black are for dinucleotide-shuffled versions of the GBS sequences. (C) Prediction of DEX-induced ChIP-reporter activity using DNA binding motifs for co-binding TFs. Responsiveness in ChIP-reporter assays was predicted using DNA motifs for TFs known to bind near or interact with the GR. Data were analyzed and plotted as above. None of the AUCs were significantly better than our null model generated using dinucleotide-shuffled sequences of the GR binding sites. (D) GR motif

strength vs. reporter density (red = DEX-induced sites, pink = dinucleotide shuffled sequences from red, black = non-DEX-induced sites, gray= dinucleotide-shuffled sequences from black). **(E)** Additive linear regression model of activity in ChIP-reporter assays predicted by overlap with TF binding sites. TF binding sites in A549 cells after treatment for 1 h with 0.02% EtOH — similar to our vehicle-control treatment — were obtained from the ENCODE project (**Table S8**). The number of called binding sites that overlapped each GR binding site from our ChIP-seq analysis was calculated. An additive linear regression model was then used to predict the estimated $\log_2(\text{fold change})$ in ChIP-reporter activity between the vehicle control library and the input ChIP-reporter plasmid library. All $\log_2(\text{fold change})$ estimates were normalized by the standard error of the estimate. Each bar indicates the corresponding regression coefficients, and the error bars are the standard error of the estimate. Stars show statistical significance, as indicated. **(F)** Additive linear regression model of DEX-responsive activity in ChIP-reporter assays predicted by overlap with TF binding sites. The data and analysis are the same as above, but predicting the $\log_2(\text{fold change})$ between DEX and EtOH treatments rather than between EtOH treatment and the plasmid input library. **(G)** Distribution of GRE motif scores among binding footprints at GR sites quantified by ChIP-exo. Motifs from elements that make up the most significant quartile of reporter expression are plotted in red and the least significant are plotted in blue. **(H)** Overlay of ChIP-exo reads for DEX-induced (blue, red) and non-DEX-induced sites (cyan, magenta). **(I)** Distribution of read depth from ChIP-exo reads per peak from DEX-induced and equal number of non-DEX-induced sites matched for read depth. Significance calculated with Wilcoxon rank sum test.

Figure S4. Related to Figure 3; Chromatin modifications and P300 occupancy at direct and tethered GBSs **(A)** Change in DNase-seq signal at sites that are DEX-induced and non-DEX-induced in ChIP-reporter assays. **(B)** Change in H3K27ac at the reporter tested GR binding sites in A549 cells after 1 h DEX treatment relative to ethanol vs. reporter fold change. Correlation coefficient factor line in solid gray. **(C)** Distribution of P300 prior to DEX exposure at among DEX-inducible and non-DEX-inducible ChIP-reporter sites at AP-1 bound and AP-1 unbound sites. **(D)** Change in H3K27me3 at the ChIP-reporter tested GR binding sites in A549 cells after 1 h DEX treatment relative to ethanol vs. reporter fold change. Correlation coefficient factor line in solid gray.

Figure S5. Related to Figure 4; GR binding clusters are nucleated by direct binding sites

(A) The number of stretches of unbound GR binding sites at 5 nM DEX (relative to possible binding sites at 50 nM DEX) is shown in blue. Sites were permuted across possible GBS locations at 50 nM DEX 1000 times. The distribution of the stretches of unbound sites in the shuffled background model is shown in red. **(B and C)** Activity as a function of GR cluster isolation thresholds. GR binding sites were assigned to local clusters based on the presence of another GR binding site within **(B)** 1 kb or **(C)** 10 kb. Mean Reporter activity is plotted as a function of number of GR binding events per local cluster. Error bars reflect the standard error of the mean (SEM) **(D)** Average Reporter activity as a function of distance between GR binding sites. GR binding sites were ordered by distance to the nearest adjacent GR binding site. The average Reporter activity was then calculated for non-overlapping windows of GR binding sites. Plotted are the average ChIP-reporter activity and average distance between sites for each window. **(E)** The fraction of GBSs that are DEX-responsive is shown as a function of the cardinality of the cluster for clustering based on a 1 kb (black), 5 kb (red), or 10 kb (blue) window. **(F-I)** The fraction of clusters with at least one DEX-responsive GBS is shown as a function of the cardinality of the cluster. Within each panel, red indicates fraction of clusters with a DEX-responsive GBS observed in our ChIP-reporter assays. Black box-plots indicate the fraction of clusters with a DEX-responsive GBS across 2000 permutations of the cluster assignments. Empirical p-values were calculated to assess whether the observed values deviate significantly from the permutations. The numbers below each column indicate (top) the upper-tail empirical p-value, (middle) the lower-tail empirical p-value, and (bottom) the number of clusters with the indicated cardinality. Each panel reports data from a different clustering window and a different significance threshold for calling a GBS DEX-responsive, as indicated in the title above each panel.

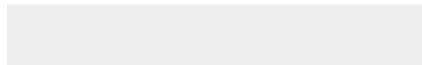
Figure S6. Related to Figure 5; Cooperative activity of tethering factors tunes the expression response to DEX. **(A)** Distribution of AP-1 motif scores calculated after dinucleotide shuffling of sites that

gained, maintained, and lost JUND binding at sites that overlap reporter active GR binding sites. **(B)** Distribution of GRE motif scores calculated after dinucleotide shuffling of sites that gained, maintained and lost JUND binding at sites that overlap reporter active GR binding sites. **(C)** Schematic of GRE/AP-1 combinatorial activation vectors used in dual luciferase assay experiments. **(D)** BAC-STARR-seq data showing the distribution of DEX-induced enhancer activity at a GR binding site proximal to the *PER1* gene on Chr. 17. Cloned GC-inducible enhancer highlighted in red. **(E)** BAC-STARR-seq data showing the distribution of GC-inducible enhancer activity at a GR binding site proximal to the *TSC22D3* gene on chromosome X. Cloned DEX-inducible enhancer highlighted in red. **(F)** Dual luciferase assays in A549 cells treated with 100 nM DEX or vehicle control performed using plasmids that contain the DEX-inducible enhancer proximal to the *TSC22D3* or *PER1* gene with combinations two proximal AP-1 binding motifs. **(G)** Dot plots showing the distribution of luciferase activity observed in GRE/AP-1 combinatorial activation experiments displayed in Figure S6F. **(H)** Schematic of vectors generated for GRE/AP-1 distal gene activation experiments. **(I)** BAC STARR-seq of neutrally acting DNA used in GRE/AP-1 distal gene activation experiments. **(J)** Dot plots showing the distribution of luciferase activity observed in GRE/AP-1 distal gene activation experiments. **(K)** Correlation (Spearman ρ +/- 1 SD) between cumulative ChIP-seq signal (log fold-change of DEX response) and gene expression, as a function of distance from TSS, for DEX-induced (blue) and non-DEX-induced (pink) GBSs.



Click here to access/download

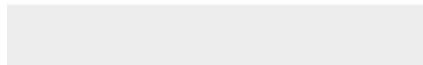
Supplemental Movies and Spreadsheets
Table_S1.xlsx





Click here to access/download

Supplemental Movies and Spreadsheets
Table_S2.xlsx





Click here to access/download

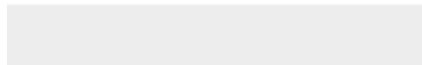
Supplemental Movies and Spreadsheets
Table_S3.xlsx





Click here to access/download

Supplemental Movies and Spreadsheets
Table_S5.xlsx





Click here to access/download

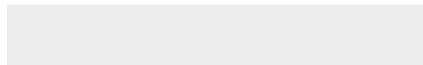
Supplemental Movies and Spreadsheets
Table_S6.xlsx





Click here to access/download

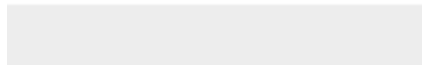
Supplemental Movies and Spreadsheets
Table_S7.xlsx





Click here to access/download

Supplemental Movies and Spreadsheets
Table_S8.xlsx





[Click here to access/download](#)

Supplemental Movies and Spreadsheets
Table_S4.xls

